Concrete cover effect on the bond of GFRP bar and concrete under static loading

Ana Veljkovic[a], Valter Carvelli[a, *], Marcin Michal Haffke[b], Matthias Pahn[b]

[a] *Department of Architecture, Built Environment and Construction Engineering, Politecnico di Milano, Piazza Leonardo da Vinci 32, 20133 Milan, Italy*
[b] *Fachgebiet Massivbau und Baukonstruktion, Technische Universität Kaiserslautern, Paul-Ehrlich-Straße, D-67663 Kaiserslautern, Germany*

Paper presents assessment of bond behaviour between GFRP bars and concrete, investigated through set of centric and eccentric pull-out specimens. Main parameters under investigation are 1) bar external surface, 2) concrete mechanical properties and 3) concrete cover. Corresponding tests with steel reinforcement are per-formed for comparison in some cases. DIC technique was used for recording and evaluating of strain field on frontal side of eccentric specimens. Consequently, cracking patterns and local bond behaviour are described in details. Increasing of concrete mechanical properties always enhanced bond strength and delayed cracking of concrete cover. Ribbed GFRP bars showed excellent bonding performance when combined with low con-crete cover. Their low splitting tendency and specific rib geometry developed better bond behaviour in case of eccentric tests, which showed the possibility of a proper prediction of the bonding behaviour of structural components.

Keywords: Glass fibres, Debonding, Mechanical testing, Concrete cover

1. Introduction

Recently developed materials present new wave of modern aspirations in construction engineering. The material that is extensively used as reinforcement of new concrete structures and strengthening of existing ones is certainly FRP (fibre reinforced polymer). Primarily developed and used in aerospace and naval industry, later on it demonstrated capability to be considered in other fields, such as construction industry. As reinforcement material, glass fibre reinforced polymers (GFRP) find increasingly more application in reinforced concrete structures. The main advantages of using GFRP reinforcement instead of steel one are: non-corrosive and non-conductive characteristics and high strength-to-weight ratio, as well as their magnetic transparency and good fatigue endurance [1]. Since first vanguard applications in last decades of XX century, new FRP reinforcement is nowadays present in many practical design codes, endeavouring to take more and more share in global usage of reinforcement for concrete structures. A considerable number of design codes and guidelines is available that treat the design procedure of FRP-RC (reinforced concrete) structures. However, they are still incomplete or very conservative due to insufficient knowledge concerning certain issues. It is well known that reinforced concrete structures require secure and balanced transfer of forces from reinforcement to surrounding concrete. Therefore, one of the most important issues in reinforced concrete design is the bond between concrete and reinforcement bar [2]. Although much research effort was spent on proper understanding the characteristics of FRP bar/concrete

bond, this area is still treated with great attention, having many aspects to research about ([3] [4]).

In the experimental investigation of reinforcement bar/concrete bond, pull-out test is well-known method that provides useful information. This wide-used, simple and cheap, but still effective method for experimental assessing of bond properties is recommended by Rilem [5]. However, fib Bulletin 10 recommends also pull-out test with eccentric placement of the bar, for estimating the concrete splitting tendency due to bond forces [6]. This test variation also simulates bar surroundings more objectively, having it positioned close to specimen side as it is in real structures. Eccentric pull-out test is conducted in this research for estimating the application possibilities of low concrete cover in combination with GFRP reinforcement. This is an important aspect in GFRP-RC structures and of relevant importance in thin RC plate elements that are usually prefabricated and used as façade panels, pavement or components of sandwich panels. Non-corrosive nature of GFRP bars and prefabrication of plate elements enable maximal lowering of the concrete cover, leaving the only concern to the correct transfer of forces through so formed bond.

From the literature, it is well-known that sanding of deformed bars improves bond performances (by equalizing or exceeding the bond strength of deformed steel rods), increases the chemical bond, but causes also brittle debonding behaviour ([7] [8]). An abrupt post-peak lowering of bond force is observed for all concrete strengths, although for lower concrete classes this behaviour is smoother [9]. Ribbed bars used in Ref. [9] presented very small unloaded-end slip and softening behaviour of after-peak curve, with some "undulations" that tend to diminish when using higher class concretes.

Low concrete cover stands in favour of FRP bars due to the softer surface, comparing to steel bars, lowering local stress concentrations in bond and delaying splitting of concrete cover [10]. Type of bar

* Corresponding author.

Email address: valter.carvelli@polimi.it (V. Carvelli)

surface determines the stress distribution in cover zone and develops the final splitting crack pattern. Sanded and helically wrapped GFRP bars showed earlier cover cracking when used with concrete of good mechanical properties [10]. GFRP bars with trapezoidal ribs showed delayed concrete cover cracking comparing to specimens reinforced with standard steel rebars [11]. Besides, concrete cover can change the failure mechanism of GFRP bar/concrete bond. Cover of one $\varnothing$ ($\varnothing$ = bar diameter) generates splitting failure mechanism, while cover of $2\varnothing$ or more, generates pull-out or fracture of the bar [12].

The mentioned and other works show a plenty of work done on static bond behaviour, but there are still some unresolved issues. Various types of FRP bars are in the market, differing in many aspects, so it is difficult to deliver global conclusions since each product has its own particular characteristics. Gathering more data about behaviour of different bar types helps in understanding this reinforcement. In this context, the present experimental investigation intends to give a contribution on the influence of some parameters affecting the bond of GFRP bar and concrete. With the aim of simulating better the real position of the bar in concrete structures, as well as assessing its cover-splitting properties, major part of specimens was designed to be eccentric, while centric ones were tested for comparison. The centric and eccentric pull-out test set-ups with GFRP and steel bars were adopted to measure the effect of: bar material and external surface, position of the bar to the element side (concrete cover) and concrete mechanical properties.

2. Materials

Two types of unidirectional E-glass FRP rebars were adopted, namely, ASLAN 100 [13] rebars of nominal diameter 6 mm and Com-BAR® [14] rebars of nominal diameter 8 mm. The GFRP rebars of both types were produced by pultrusion technique with vinyl-ester resin. Those of diameter 6 mm have surface deformed with helical wrap and coated with coarse sand, while 8 mm rebars have external ribbed surface cut into the bar after curing (Fig. 1). Table 1 contains the mechanical properties of the rebars in the direction of the bar axis, according to the data sheet of the producers.

For the sake of comparison, tests were carried out with conventional steel ribbed rebars (grade B500B, Table 1) of the same nominal diameters (6 and 8 mm).

For assessing the bond behaviour, contact surface area was calculated using the nominal diameter in case of ribbed bars -

ComBAR® and steel ones. For sanded and wrapped GFRP bar of nominal diameter 6 mm, diameter equal to 6.35 mm was used for calculating the bond contact area, according to the product catalogue [13] and ACI440.3R [15].

Regarding bar surface treatment, same type of sanded and helically wrapped GFRP bars and same concrete strength (approx. 50 MPa) were used in Ref. [9] that reported abrupt decay in bond strength after the peak stress for small bar diameters. Here, bar with diameter of 6 mm is expected to show similar behaviour.

As for ribbed steel bars, Fib Bulletin 10 [6] gives an index to incorporate the properties of the rib geometry. The ''bond index'' or "relative rib area" f_b is given by:

$$ f_b = \frac{A_R}{\pi \cdot d_b \cdot s_R} \tag{1} $$

where A_R, d_b and s_R are area of the projection of a single rib on the cross-section, bar diameter and rib spacing, respectively.

It should take values between 0.05 and 0.10 for a good compromise in terms of bond strength, splitting forces and limitation of crack width [6].

Optimal rib spacing is equal to the rebar diameter, optimal rib height is 6% of the rebar diameter, and corresponding relative rib area of the rebar is 0.06 [16]. Optimum rib width recommended for similar conditions is 5.36 mm [17]. The selected type of ribbed GFRP bar (ComBAR, diameter 8) has rib spacing, height and width 8.12 mm, 0.49 mm and 5.43 mm, respectively, which provide a bond index $f_b = 0.064$, corresponding to the recommendations. In case of steel bars, fib Bulletin 1 [18] prescribes relative rib area of 0.039, i.e. 0.045 for bar of diameter 6, i.e. 8, respectively [18]. Selected steel bars correspond to these recommendations, following [19].

In total, four different concrete classes were used, named C1, C2, C3 and C4. Table 2 lists the components content of each concrete mix.

The compressive and tensile strength of the concrete, as well as compressive modulus of elasticity, were experimentally determined for each concrete mixture. Samples for mechanical properties' tests were cast at the same time as pull-out specimens, kept in formwork 24 h and afterwards in the same laboratory conditions as pull-out specimens, with constant temperature and humidity of the air. Cubic specimens (150 × 150 mm) were used for determining compressive strength [20] and cylindrical ones (150 × 300 mm) for tensile strength [21] and compressive modulus of elasticity [22]. Average compressive cubic strengths, tensile strengths and moduli of concretes are listed in Table 3.

Fig. 1. Surface of the GFRP rebars: (a) ASLAN 100, Ø 6 mm; (b) ComBAR, Ø 8 mm.

Table 1
Mechanical properties of bars (*yield strength of steel bars).

GFRP Bar	Nominal diameter [mm]	External surface	Tensile strength [MPa]	Tensile modulus of elasticity [GPa]
ASLAN 100	6	Wrapped, sanded	896	46
ComBAR®	8	Ribbed	1500	60
Standard steel rebar B500B	6 and 8	/	500*	210

Table 2
Specification of the concretes mixes.

	Concrete ID			
	C1	C2	C3	C4
Water [kg/m³]	184	177	195	188
Cement CEM I 42,5 N [kg/m³]	255	295	510	450
w/c ratio	0.72	0.60	0.38	0.42
Fine aggregate 0/2 mm [kg/m³]	838	509	739	525
Medium aggregate 2/8 mm [kg/m³]	1011	617	895	580
Coarse aggregate 8/16 mm [kg/m³]	–	–	–	530
Superplasticizer ACE 30 BASF Master Glenium FM 794 [kg/m³]	–	–	2.27	2.03

Table 3
Mechanical characteristics of the considered concretes.

Concrete ID	Compressive cubic strength		Tensile strength		Compressive modulus of elasticity	
	Average [MPa]	St. Dev. [MPa]	Average [MPa]	St. Dev. [MPa]	Average [GPa]	St. Dev. [GPa]
C1	23.3	1.1	2.29	0.19	19.71	1.07
C2	38.9	2.7	3.32	0.48	22.45	0.81
C3	56.3	2.8	3.96	0.27	27.88	0.53
C4	62.3	4.3	n.a.	n.a.	n.a.	n.a.

3. Specimens and experimental setup

The experimental campaign comprised of eccentric, as well as typical centric pull-out tests. The geometry of the former was slightly modified comparing to suggestions of fib Bulletin 10 [6]. Centric specimens were cubic with the 200 mm edge, while eccentric specimens had dimensions 200 × 200 × 150 mm (see Fig. 2a, b). Fib Bulletin 10 [6] suggests the height of the eccentric specimens to be equal to the size of bond length of the bar. In this research, eccentric specimens had height of 200 mm, therefore approximately 6 times bigger than embedment length, which was positioned at the upper part of the specimen. Such layout helps to lower the impact of contact between concrete and support steel plate on the bond zone and enables comparing with standard centric pull-out tests. The eccentric specimens did not have cubic shape, but one side slightly shortened, to allow proper positioning in the loading frame. Specimen geometry and relative bar position are shown in Fig. 2a, b, where l is the bar free length from the bond zone to the grip tabs, $\varnothing$ is the bar nominal diameter and c is the concrete cover. The rebars were embedded in specimens to provide three concrete covers: 10, 15 and 20 mm. Centric bar configuration was considered for comparison. The bond length between bar and concrete was selected as $5\varnothing$, inserting an aluminium pipe on the bar. Aluminium pipe prevented forming of bond between concrete and the bar along the bond-free length.

The bars had horizontal position during specimens casting, being orthogonal to the direction of concrete pouring. The casting layout provided flat and even surface of the concrete block side that is relying on bottom steel plate of the testing frame. Therefore, the pressure transfer from concrete block to steel plate was supposed uniform.

Specimens were cast in wooden moulds, covered 24 h with plastic foil for curing, after which the formwork was taken off.

Pull-out specimens were named as: first letter stands for a bar type (G = GFRP, S = Steel), followed by bar diameter (6 and 8 mm), concrete type (C1 – C4, as given in Table 2) and bar position (c = centric, 20 mm, 15 mm and 10 mm for corresponding concrete covers). E.g., G8C3_20 implies GFRP bar of diameter 8 mm, cast in concrete C3, having a concrete cover of 20 mm. Table 4 lists all combinations of mentioned parameters considered in this experimental campaign.

Steel testing frame had significant stiffness to provide adequate rigidity of the setup during loading Fig. 2c.

PTFE (PolyTetraFluoroEthylene) sheet was positioned between concrete specimen and steel frame bottom plate in order to lower the influence of friction forces on the stress state in the concrete surrounding the bar. PTFE layer allowed the dilatation of the concrete in the plane of contact, diminishing the excessive forces to arise in concrete block. Special cylindrical sleeve was gripping the bars with three-piece wedge that transferred the load without damaging the bar in the gripping section.

Three specimens were tested quasi-statically for each considered combination. The total number of specimens tested was 51.

The quasi-static pull-out tests were performed displacement-controlled, in order to get the additional information about the post-peak bond behaviour. Crosshead displacement rate was set to 1 mm/min
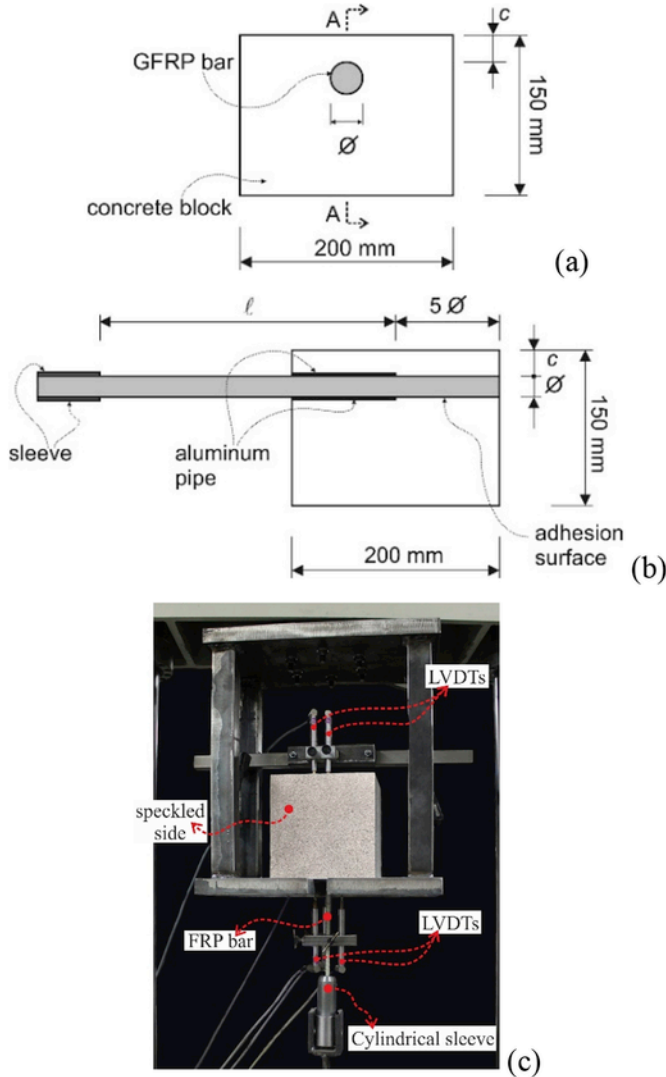

Fig. 2. Eccentric pull-out specimen geometry: (a) top view; (b) longitudinal section A-A. (c) Experimental setup.

Table 4
Overview of performed tests and specimen ID.

Concrete ID	Bar material	Bar diameter [mm]	Concrete cover [mm]	Specimen ID
C1	GFRP	8	10, 20, center	G8C1_10, _20, _c
C2	GFRP	8	10, 20, center	G8C2_10, _20, _c
C3	GFRP	8	10, 20, center	G8C3_10, _20, _c
C4	GFRP	6	15, 20	G6C4_15, _20
	GFRP	8	10, 15, 20	G8C4_10, _15, _20
	Steel	6	20	S6C4_20
	Steel	8	10, 20	S8C4_10, _20

and the tests were stopped when bond stress was lower than 10% of its maximum value.

Two LVDTs (linear variable displacement transducers) were placed on the top of the cube to continuously measure displacement: one of the bar and another of the concrete surface next to the bar. The difference of these displacements provides the slip between the bar and the concrete. LVDTs were continuously recording the slip, with acquisition frequency of 1 Hz. Three bottom LVDTs were used to measure bar loaded-end displacement for accessing the bond-damage development process. They were positioned uniformly with a distance of 120° between each other around the bar. The mean value of recorded displacements gave precise results, eliminating effects of possible bar/instruments inclination. Elastic elongation of the bar was subtracted from raw values, giving data related only to the slip at the beginning of the bond part.

For this kind of experiments, strain data on the specimen front surface is usually collected by applying strain gauges on the area of interest. In the present case, information about the strain on the specimen side close to the bar was obtained by DIC (digital image correlation) method [23]. The DIC method is non-contact technique capable to provide the measurement of the full field displacement and the calculation of full field strain on the external surface of the sample during loading. Accordingly, some quasi-static tests were assisted with two digital cameras acquiring frames at frequency of 1 Hz with a resolution of 2448 × 2050 pixels. The post-processing of images allowed the measurement of the 3D full field displacement on front side of the specimen by the 3D digital image correlation technique using the ARAMIS software [24]. For this purpose, that side of the specimen was white painted and randomly speckled with black acrylic paint.

4. Results and discussions

The results were examined considering: bond stress (τ) – slip curves, bond strength, corresponding slip values and damage mechanisms. Assuming constant shear stress (τ) along the contact surface between bar and concrete, τ vs. slip curves were compared for assessing the influence of: bar external surface and material, bar diameter, concrete and cover. Curves were constructed for both, free-end and loaded-end slip values. Strength and slip values were compared through histograms, while debonding and cracking mech-

anism were described using naked-eye inspections and DIC analysis of the full-filed strain patterns.

4.1. Influence of bar properties

The advantages and drawbacks of both types of GFRP bars were emphasized comparing to commonly used standard steel reinforcement bars. For that purpose, one concrete type was selected (concrete C4) and different concrete covers: three for GFRP bars (10, 15 and 20 mm) and two for steel bars (10 and 20 mm). Each type of GFRP bar is compared to steel bar of corresponding diameter. Direct comparison of two types of GFRP bar cannot be made because bars are of different diameters, so since the cover values are constant, ratio cover/bar diameter is different.

Fig. 3 shows typical τ – free-end slip diagrams for each bar type and concrete cover. For concrete covers of 15 and 20 mm, GFRP bar $\varnothing 6$ had characteristic post-peak behaviour (Fig. 3a), with an abrupt drop of shear stress after reaching its maximum value (see curves named 'mode A'). The same was already observed using centric pull-out tests in Refs. [9] and [17], but for a different bar type (sand coated bars and sparsely ribbed bars, respectively). During the phase of sudden drop of bond stress, sanded external surface of the bar was completely detached from the bar core. The load drops from maximum to almost zero, while the slip increases for almost 4 mm. After complete debonding, the bar establishes a friction-based bond mechanism. Consequently, the bond stress increases up to the value of 10.5 MPa, then the free-end of the bar starts to slip again. After sanded external layer is peeled off, the bond resistance is based on reduced friction between bar core and its external layer. Such bond stress is slowly and gradually decreasing as the embedded length is becoming smaller [25]. However, equally obtained for both covers (15 and 20 mm) is another type of τ – free-end slip curve, with different post-peak behaviour (named 'mode B' in Fig. 3a). These curves showed friction controlled, moderately steep descending branches (Fig. 3a). After reaching a slip of almost 5 mm, both types of bond mechanism have the same friction based bond resistance. The second type of curve (mode B) always attained slightly lower bond strength comparing to firstly mentioned one (mode A), although the final failure mode was the same (shearing off the surface deformations of the bar). The only difference was that mode B started bar debonding at lower stress level, subsequently followed by slip growth that engaged bond frictional resistance. In this way, the abrupt loss
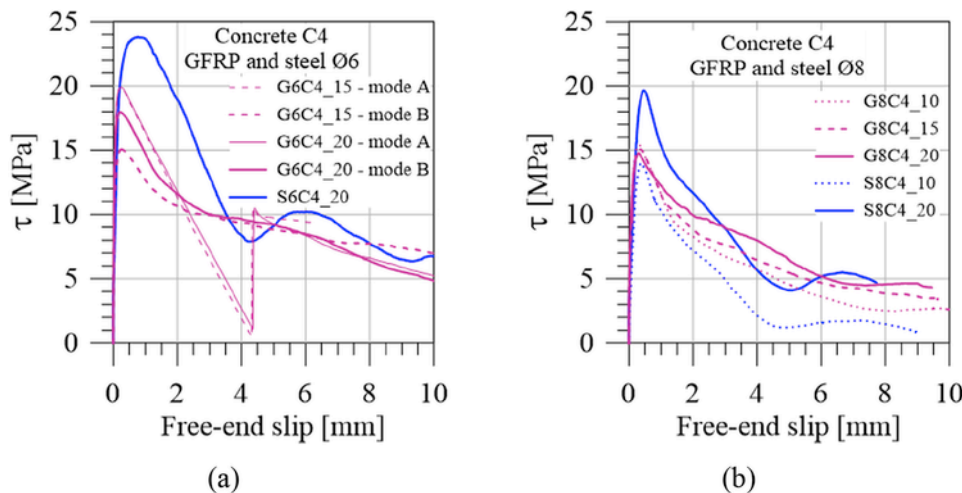

Fig. 3. Typical τ-slip diagrams of bar (a) $\varnothing 6$ - GFRP and steel; (b) $\varnothing 8$ - GFRP and steel, embedded in concrete C4 with concrete cover of 10, 15 and 20 mm.

and re-establishment of bond stress was avoided and force transfer remained continuous.

The mentioned bond behaviour can be analysed considering the measurements of the DIC (Fig. 4). Captured area of photos analysed by DIC system is positioned in the middle top part of the specimen's front side, encompassing embedment length of the bar together with its surroundings. Fig. 4 presents crack pattern development through some selected stress levels in pre-peak and post-peak phase. Cracks start appearing on the specimen front side from the shear stress level of 11 MPa and they are clearly distinguished at 13 MPa, for both analysed failure modes (first column in Fig. 4). The 15 MPa maps show crack condition at maximum bond stress level for 'mode B' specimen. The map for 19.9 MPa represents the strain distribution at the bond strength level of 'mode A' specimen. This is not available for 'mode B' counterpart, having lower maximum stress level. Most right column in Fig. 4 shows crack condition at post-peak bond stress level of 10 MPa. The DIC results allow better understanding of the bond failure modes. Namely, during the pre-peak phase, splitting crack starts to develop from the bottom of embedment length in case of both failure modes (A and B). Along with this, interlaminar bond between core of the bar and its outer layer is weakening while transferring the shear stress from the bar to concrete. Specimens having an abrupt post-peak stress reduction ('mode A'), had a cover crack all along the embedment length when the maximum load was reached (Fig. 4, 19.9 MPa), while for 'mode B' failure, DIC analysis showed that at the maximum bond stress main cover crack still did not reach the top edge of the specimen (Fig. 4, 15 MPa, bottom row). This indicates that in case of 'mode B' the bond capacity of the bar decreased by internal delamination before complete splitting of cover. Afterwards, when bond stress started to decrease and slip to increase, final crack pattern developed reaching the top edge of the specimen (Fig. 4). On this way, the abrupt loss and establishment of bond stress was avoided and the force was smoothly and continuously transferred. Opposite to that, specimens of 'mode A' underwent typical cover crack induced failure. Subsequently, interlaminar bond broke, as being already weakened, and sand layer maintained attached to its concrete surroundings. Since essential confinement was lost, bond

stress decreased abruptly, but became re-established by residual friction. Essentially, the main difference between these two failure modes is the splitting crack pattern governing the first part of post-peak bond behaviour.

The same occurrence was observed for 20 mm cover (Fig. 3a).

Particular reason for occurring these two different bond mechanisms (mode A and mode B) is attributed to the local influence of bar surface deformations. Namely, spiral winding pitch of GFRP rebars ⌀6 was around 20 mm, and embedment length was selected as $5\varnothing = 30$ mm, therefore insufficiently to encompass uniform distribution of surface deformations, as also reported in Ref. [26]. Such setup led to more pronounced local influence of specific bar part within the embedment length, which caused different distribution of bond forces and non-uniform debonding behaviour. Therefore, the combination of bar surface, bond length and concrete covers created a transition condition between the two failure modes.

In case of 20 mm cover for steel bar ⌀6 (Fig. 3a), curve shows higher peak stress, small plateau at peak and abrupt descending brunch. After reaching slip of almost 4 mm, it shows 'undulating behaviour' caused by stiff steel ribs encountering the re-engaged mechanical interlock after shearing off the concrete lugs, as already reported for steel bars in Refs. [9] and [27].

GFRP bar diameter 8 mm (Fig. 3b) with cover of 10 mm had descending branch composed of two parts distinguishable mainly for the slopes. The variation of slope was approximately for a slip of 1.5 mm, which represent the end of abrupt cracking of concrete corbels between bar ribs and start of debonding phase, being based only on friction between bar and concrete. Therefore, after exploiting mechanical bearing capacities of bond, following stage is based on residual friction between bar and concrete interfaces and possibly interlaminar debonding, since photos of the bar taken after pull-out process showed some damage on the bar surface (Fig. 11). Diagram for specimen with steel bar distinguishes also two parts in descending branch, having similar mechanism as reported for GFRP bar ⌀8 mm. First part has the larger slope which decreases reaching approximately 5 mm of slip and 20% of maximum bond strength. After this, curve has typical 'undulating' behaviour, as mentioned above for
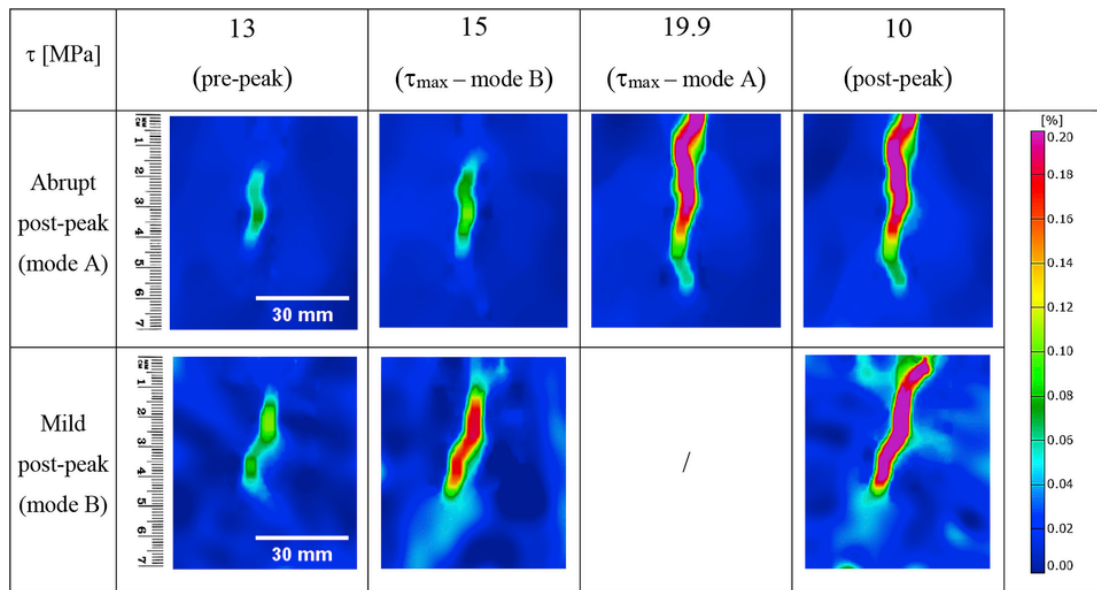

Fig. 4. Contour plots of the maximum principal strain captured on the front side of specimens G6C4_15 (GFRP ⌀6 with 15 mm cover). Upper row G6C4_15 – mode A, bottom row G6C4_15 – mode B.

steel bar of diameter 6 mm. GFRP bar has similar, but less pronounced behaviour due to the bar low modulus of elasticity especially in radial direction, enabling similar deformation of the two materials at the interface and more gradual debonding than steel bars.

Overall, regarding high strength concrete (C4) and 10 mm concrete cover, no relevant difference between GFRP and steel bars of diameter 8 mm can be mentioned (Fig. 3b). An advantage of GFRP bars is related to the better post-peak branch, requiring almost 30% more energy during debonding process. Bond energy was calculated as the area under τ – free-end slip curves, in the range of 0–7 mm. Its average value is 57.2 MPa*mm and 41.3 MPa*mm for GFRP and steel bars $\varnothing 8$, respectively.

Fig. 5 presents strain maps comparison, by DIC, at different stress levels of the pull-out process of steel and GFRP $\varnothing 8$ embedded in concrete C4 and concrete cover of 10 mm. Both systems attained similar bond strength. Patterns clearly show that GFRP bar starts developing splitting crack for a higher load level than the steel one. At load levels close to 3.7 MPa (considered the design bond stress of the bar producer [14]), GFRP develops only diffused smeared cracking pattern, while steel bar already starts to form main splitting crack that in the end caused bond failure at ultimate load level.

Raising the load, both bars create main splitting crack starting from the bottom of embedment length, and then spreading upwards and downwards. Both bars develop progressive bond failure mode, although the embedded length is fairly small. Final failure takes place when crack reaches top edge of the specimen (Fig. 5, right columns, maximum shear stress 14 and 15.4 MPa for steel and GFRP bar, respectively), thus completely disabling confining effect of surrounding concrete and 'cover crack' failure occurs.

However, concrete corbels, still attached to the bar surface, are still 'working' after reaching peak stress and until bond starts to rely only on friction. Therefore, the decrease of post-peak stress is not as abrupt as in case of cover cracking failure with sanded and spirally wrapped bars, previously described. Along with main crack, additional side cracks appear during debonding process, due to still present mechanical action of bond. In case of GFRP bar none of them

reaches the very edge of the specimen up to the end of bar pull-out process, as in case of steel. This is supported by pictures showing the crack pattern from top of the specimens, accompanied with DIC maps of the front side, taken at the end of pull-out process (Fig. 6). Steel bars create more extended damage during debonding process. The wider concrete corbels on steel bars (Fig. 11) require more fracture energy for failure, leading to extensively cracked concrete cover and reduction of the residual friction of bond. Opposite to this, GFRP bars $\varnothing 8$ have narrow corbels, which produce less damage of the cover and allow higher frictional capacity of the bond comparing to steel bars. This explains higher fracture energy needed for debonding of the GFRP bars, as stated previously.

The curves in Fig. 3b, for GFRP bars $\varnothing 8$ with 15 and 20 mm covers, are fairly similar to the one with 10 mm cover. Furthermore, steel bar of diameter 8 mm has similar bond behaviour for cover 20 mm, as for cover 10 mm.

For concrete cover of 20 mm, the post-peak branch of the GFRP bar specimen has slope more gradually decreasing then steel one, which shows the typical two parts.

Strain maps for concrete cover of 20 mm, in Fig. 7, show that GFRP bar starts developing major splitting crack at lower load level, comparing to steel bar, but towards higher stresses they attain similar pattern. The onset of the crack at the surface starts for a significantly higher stress comparing to 10 mm cover. Failure mode is again progressive, for both bar types, and bond failure occurs due to cover crack, when it reaches top edge of the specimen (Fig. 7, right column, maximum shear stress 19 MPa).

GFRP bar of 6 mm diameter with cover of 20 mm has lower average bond strength than the steel counterpart (Fig. 8a). GFRP and steel bars of diameter 8 mm have comparable bond strength for cover 10 mm (Fig. 8b), while steel bar has almost 20% higher strength for cover of 20 mm. Having in mind that FRP bars develop lower splitting forces than steel bars [10], the benefit of using of GFRP bars is particularly visible for low concrete covers (10 mm in this case).

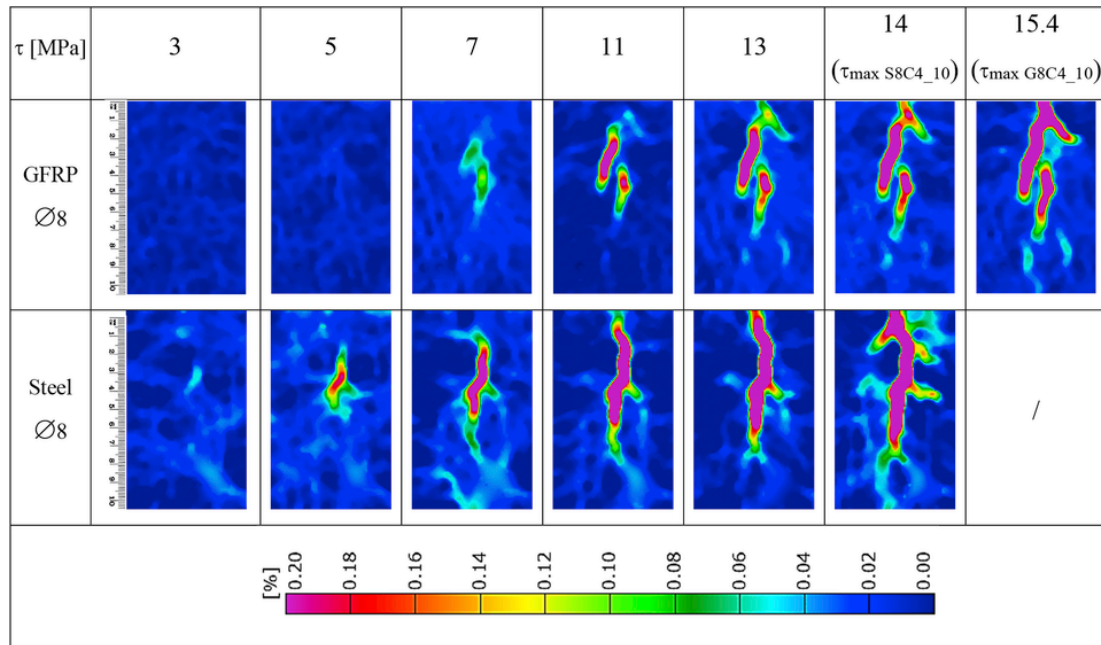The free-end-bar slip for maximum value of bond stress is generally smaller for GFRP bars than for steel ones. GFRP bars $\varnothing 6$

Fig. 5. Maximum principal strain map at different τ levels. Crack evolution for steel and GFRP ∅8 bar embedded in concrete C4, with concrete cover of 10 mm.
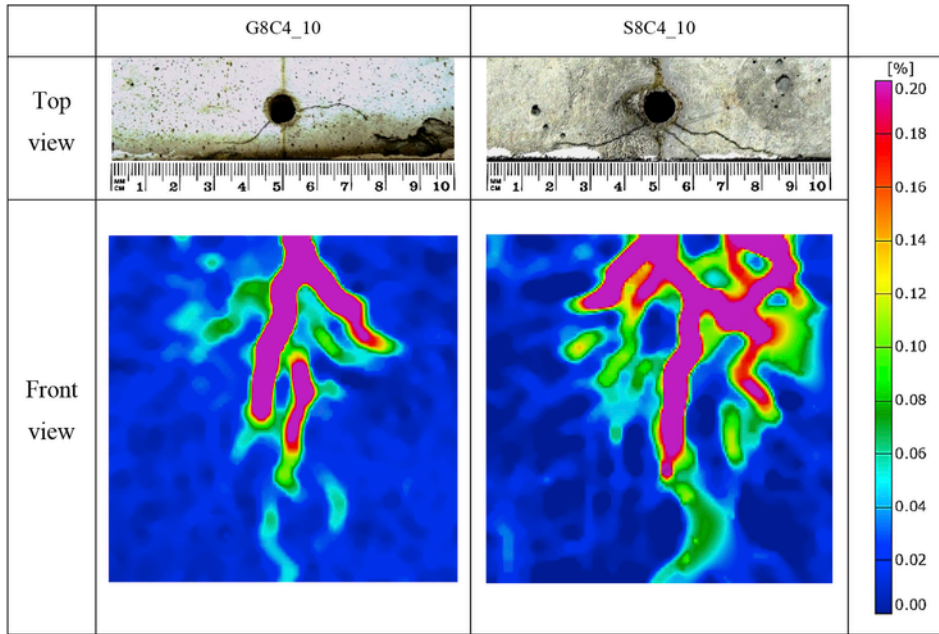
Fig. 6. Cracks pattern at the end of pull-out process, for GFRP and steel bar ∅8 embedded in concrete C4, with concrete cover of 10 mm, top side naked-eye view and front side DIC maximum principal strain map.
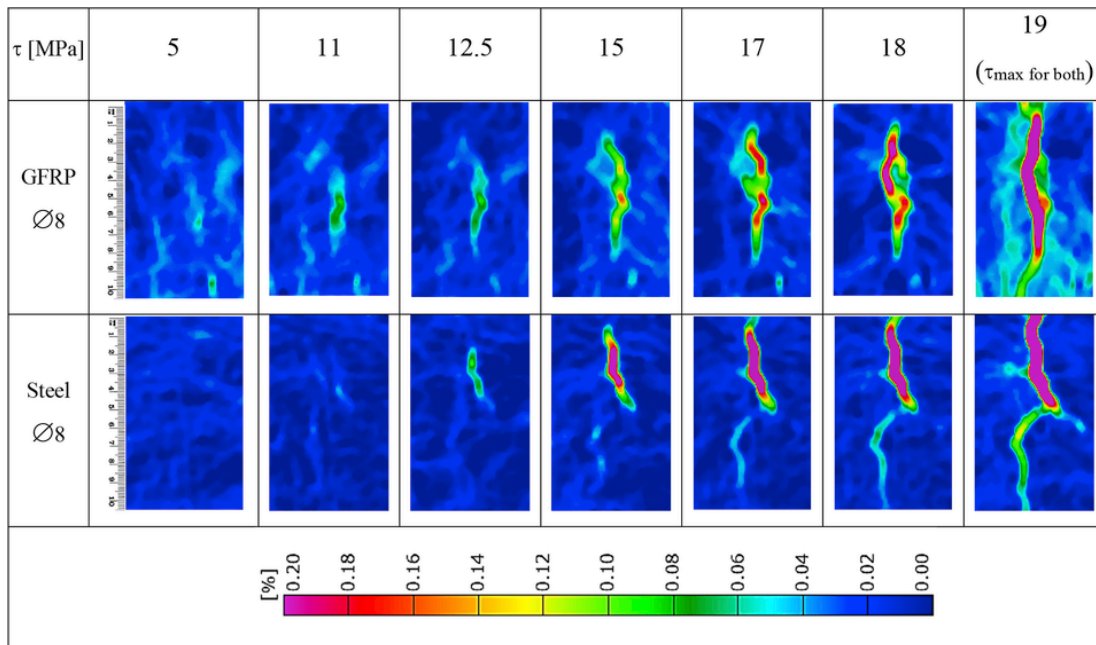

Fig. 7. Maximum principal strain map at different τ levels. Crack evolution for GFRP and steel ∅8 bar embedded in concrete C4, with concrete cover of 20 mm.

showed the smallest values overall, and especially comparing to steel bars, which have almost triple average slip value in case of 20 mm concrete cover (Fig. 9a). Generally, GFRP bar ∅6 free-end slip has a value of about 0.2 mm with high concrete strength and covers of 15 and 20 mm (Fig. 9a). This stiff bond behaviour is not surprising for sanded and wrapped GFRP bars, being already reported [7].

Ribbed GFRP bars ∅8 demonstrated higher bar slips for maximum value of bond stress, compared to sanded and wrapped ∅6 bars, but slightly smaller compared to steel. Their values range from 0.3 to 0.4 mm (Fig. 9b). Since failure mode of GFRP and steel

bars ∅8 is quite similar, and having in mind lower width of concrete corbels in case of GFRP (Fig. 11), it is expected that they start cracking at moderately lower slip level compared to steel. Nevertheless, these GFRP bars develop bond strength quite comparable to steel bars of same diameter and peak bond stress is reached at similar slip values. The difference is failure mechanism. Concrete corbels in contact with GFRP bar, defined by bars' external rib surface, shear off along the plane parallel to bar axis and stay compact till the end of pull-out process. Opposite to that, corbels in contact with steel bar are crushed diagonally and stacked in front of bar lugs, enhancing radial
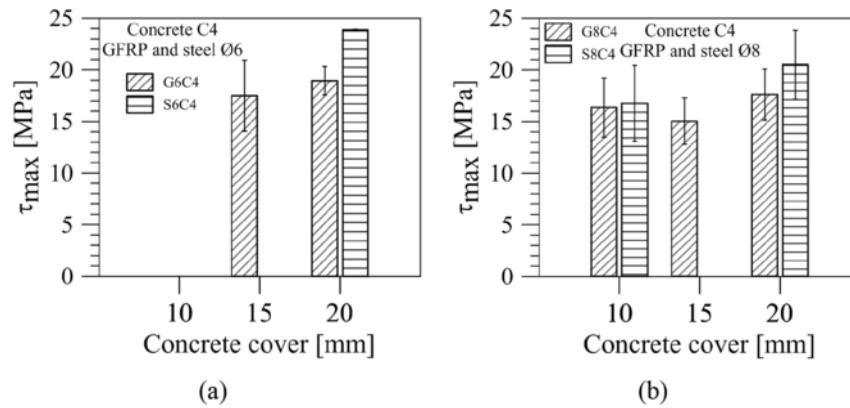
Fig. 8. Bond strength of bar (a) Ø6 - GFRP and steel; (b) Ø8 - GFRP and steel, embedded in concrete C4. Average and standard deviations (error bars) of three specimens.
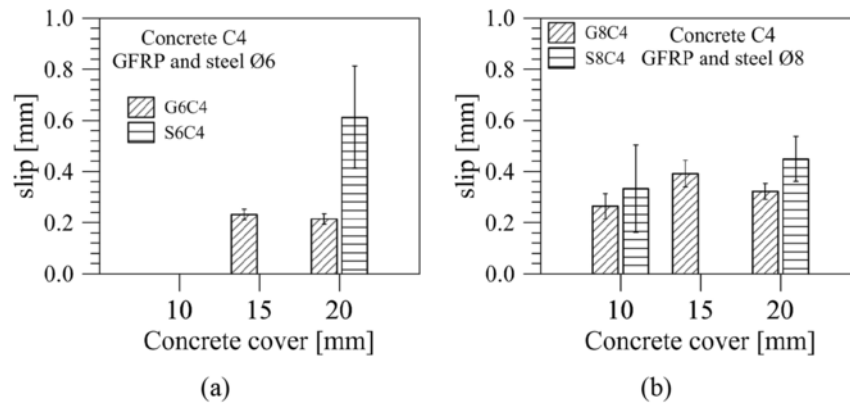
Fig. 9. Free-end slip at maximum bond stress of bar (a) Ø6 - GFRP and steel; (b) Ø8 - GFRP and steel, embedded in concrete C4 with concrete cover of 10, 15 and 20 mm. Average and standard deviations (error bars) of three specimens.

component of bond stress and consequently splitting of concrete [6] by changing the bond force angle. This happens because the corbels in contact with steel bar have shear surface bigger than those in contact with GFRP bar. So, although stress and slip parameters are similar, debonding mechanism is slightly different.

Bar external surfaces were deeply observed before and after pull-out process. In case of GFRP bars Ø6, failure occurs due to total delamination of FRP external surface, including sand and part of the fibres squeezed out by wrapping (Fig. 10). This occurs for all covers.

Fig. 10. Surface of GFRP bar of diameter 6 mm, concrete C4, after pull-out.

Damage mechanism of bond between steel bar and concrete is typical, for all diameters and covers, crushing of concrete without any damage of the bar.

GFRP bars of diameter 8 mm, with cover of 10 mm, had, as main damage mechanism, shearing off the concrete corbels in between bar ribs. Some damage was noticed on the bar surface, as well, in the form of slight grooves (Fig. 11).

For other two values of covers (15 and 20 mm), crushing of concrete corbels, with scratched bar surfaces, were observed, similarly as for cover of 10 mm.

4.2. Influence of concrete strength

The influence of the concrete mechanical properties was investigated for the considered 4 concrete types in combination with GFRP bar of diameter 8 mm, different concrete covers (10 and 20 mm) and the bar in the center.

Fig. 11. Surface of (a) GFRP and (b) steel bar of diameter 8 mm, concrete C4 and cover 10 mm, after pull-out.

Fig. 12 shows typical τ – free-end slip diagrams, while Fig. 13 shows corresponding τ – loaded-end slip diagrams, considering all mentioned parameters.

As mentioned, the post-peak branch is composed of two parts with different slopes. The lower strength concretes demonstrated more slow and continuous decreasing of slope after peak, that was even more pronounced in case of centric specimens. Therefore, lower strength concretes produce less brittle bond behaviour as confinement of the bar is increasing.

τ – loaded-end slip curves follow the shape of their free-end counterparts. The initial slope of their ascending branches gives the initial bond stiffness that is higher in case of the higher concrete qualities (Fig. 13). Better insight in the relation between free- and loaded-end slip is given by diagrams in Fig. 14. The comparison shows the difference between the loaded- and the free-end slips. Having in mind that the difference is very sensitive to bar modulus of elasticity (not experimentally measured), its absolute value was not considered relevant, but only the variation along with bar slipping. Diagrams in Fig.
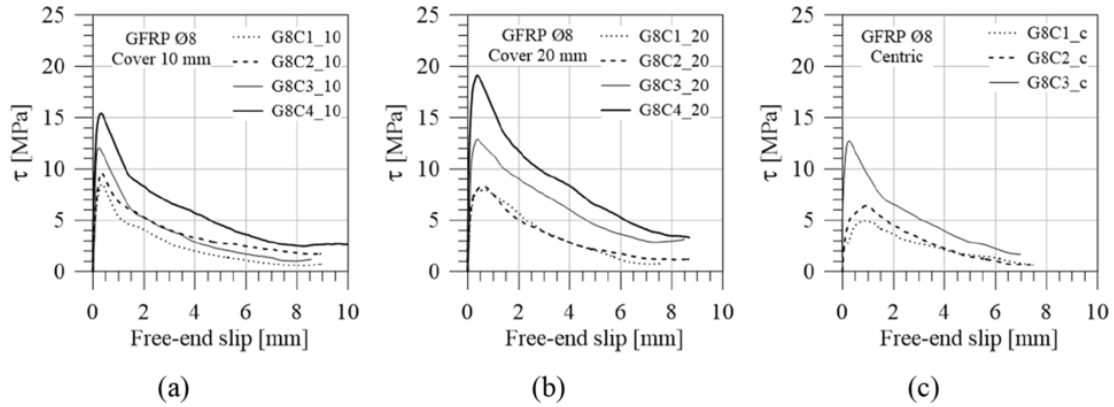
Fig. 12. Typical τ - free-end slip diagrams for GFRP bars ⌀8 embedded in concretes C1-C4 for concrete cover of (a) 10 mm, (b) 20 mm and (c) centric.
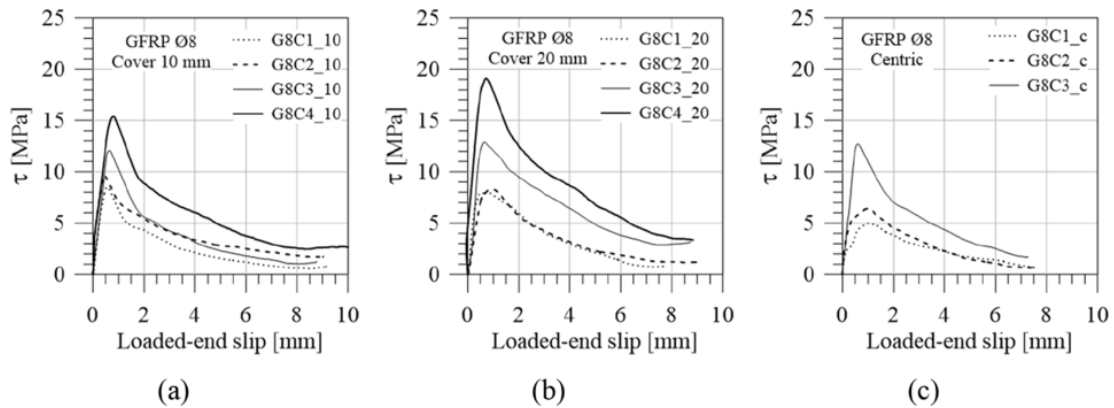
Fig. 13. Typical τ - loaded-end slip diagrams for GFRP bars ⌀8 embedded in concretes C1-C4 for concrete cover of (a) 10 mm, (b) 20 mm and (c) centric.
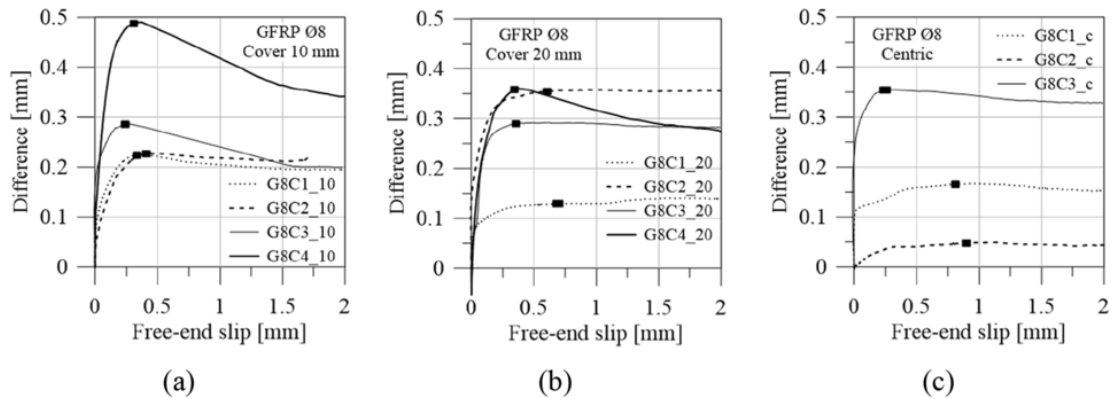
Fig. 14. Typical diagrams showing the difference between loaded-end and free-end slip for GFRP bars ⌀8 embedded in concretes C1-C4 for concrete cover of (a) 10 mm, (b) 20 mm and (c) centric. Square symbols correspond to slip values at maximum bond stress.

14 have square symbols corresponding to bond strength, as a reference for assessing the debonding process. Looking at the very low slip value range in Fig. 14, higher strength concretes (C3 and C4) develop continuous increase of the loaded-end slip, as indicator of progressive failure mode [28]. Unlike them, lower strength concretes (C1 and C2) have less sharp slope of the ascending curve branch.

Fig. 15 shows bond strength increasing trend with improving the concrete quality, for all three confinements. C1 and C2, which have average cubic compressive strength of 23.3 MPa and 38.9 MPa, generate almost the same value of bond strength. There is a relevant improvement of the bond strength from concrete C2 (38.9 MPa) to C3 (56.3 MPa), while the reduced difference of compressive strength between concrete C3 and C4 (56.3 MPa and 62.3 MPa, respectively) provides significant increase of bond strength of 25% and 21% for cover of 10 and 20 mm.

The free-end-bar slip for maximum value of bond stress has reverse trend comparing to bond strength values (Fig. 16). A sudden decrease of slip was recorded in the transition between C2 and C3, and similar slips occurred for higher strength concretes (C3 and C4). The difference of slip between these two concrete groups (lower and higher strengths) is about 25% for 10 mm cover, 45% for 20 mm cover and 40% for centric specimens. Therefore, especially in case of lower strength concrete, the combination with lower cover value would result in optimal solution for achieving good bond properties.

The influence of the concrete class on the failure mode of specimens with GFRP bar is detailed in Fig. 17. With increasing the concrete quality, the quantity of residual concrete between bar ribs increases. The imprints in concrete reveal that as the concrete compressive strength becomes bigger, the pattern of the bar is more distinguished (especially in case of 10 and 20 mm cover) and fibres detached from bar surface are also more visible (Fig. 17).

As shown by the cracks' development pattern (Figs. 5, 7 and 18), the stress level for crack initiation increases with the concrete strength, for both covers of 10 and 20 mm. For 10 mm cover crack appears at stress level of 2–3 MPa for concrete C1 (Fig. 18), while for C4 it appears at 7 MPa (Fig. 5). In case of 20 mm cover, the initiation stress ranges from 5 MPa to 11 MPa for concretes C1 and C4, respectively (Figs. 7, 18).

Top view of specimens after pull-out revealed splitting of concrete surrounding the bar (Fig. 19). From lowest to highest strength concrete, the cracks' angle becomes sharper, causing longer crack paths and wider concrete area resisting splitting, and generally higher resistance to failure. However, concrete C4 does not follow this behaviour. The reason is likely due to the high concrete strength, which is less prone to "plasticization" [10].

4.3. Influence of the concrete cover

The influence of concrete cover is very important since the possibility of concrete cover reduction allows full utilization of excellent chemical resistance of FRP bars. Therefore, special attention of this work is put on the possibilities to maximally lower the cover value, simultaneously providing secure bonding conditions.

The comparison was made for GFRP ⌀8 bar in combination with concretes C1 - C4, including cover of 10 and 20 mm, as well as 100 mm (centrically positioned bars in specimens).

The main effect is visible analysing the bond strength in Fig. 15. The bond strength slightly decreases for concretes C1 – C3, and in-
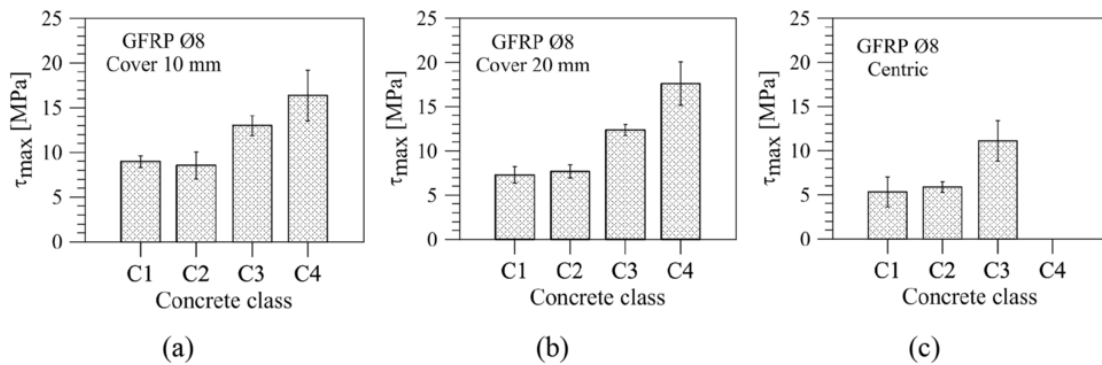

Fig. 15. Bond strength of GFRP bar ⌀8 embedded in concrete C1-C4 with cover of (a) 10 mm, (b) 20 mm and (c) centric. Average and standard deviations (error bars) of three specimens.
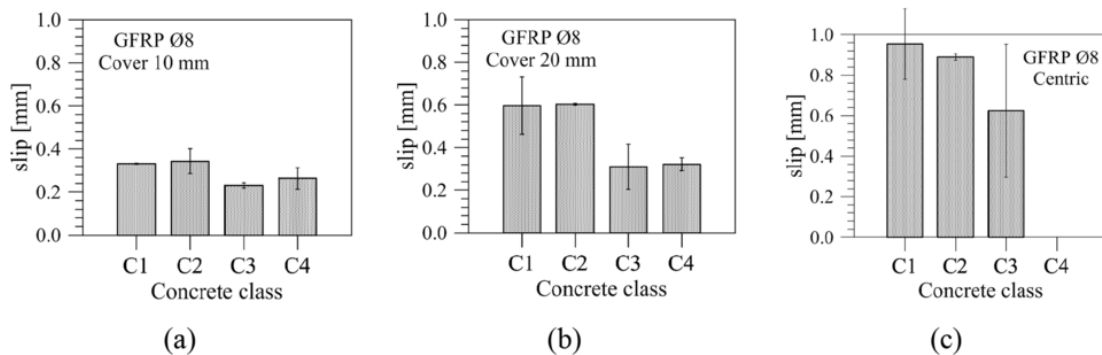

Fig. 16. Free-end slip at maximum bond stress of GFRP bar ⌀8 embedded in concrete C1-C4 with cover of (a) 10 mm, (b) 20 mm and centric. Average and standard deviations (error bars) of three specimens.
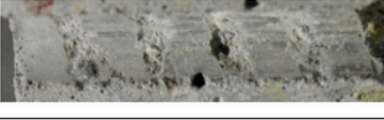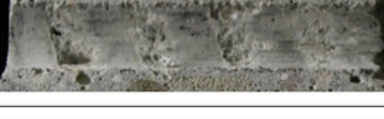
Concrete ID	Concrete cover	Bar surface	Concrete surface
C1	10 mm		
	20 mm		
	centric		
C3	10 mm		
	20 mm		
	centric		

Fig. 17. Surface of GFRP bar of diameter 8 mm (left) and imprints in concrete (right), for concrete qualities C1 and C3.
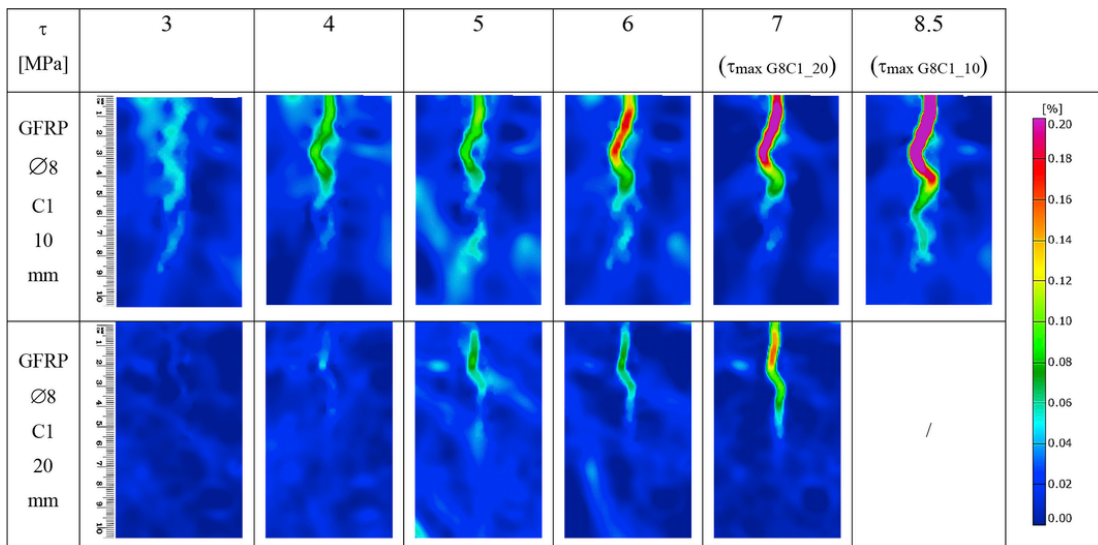

Fig. 18. Maximum principal strain map at different τ levels. Crack evolution for GFRP ∅8 bar embedded in concrete C1, with concrete cover of 10 and 20 mm.

creases for C4, when concrete cover raises from 10 to 20 mm. But, comparing centric to 10 and 20 mm cover specimens, the bond strength is lowered about 30% for concretes C1 and C2 and 15% for concrete C3. Also, with increasing of confinement, specimens have larger slip values at maximum bond stress (Fig. 16).

Those observations indicate that GFRP bar of diameter 8 investigated in this research shows better bond characteristics in case of
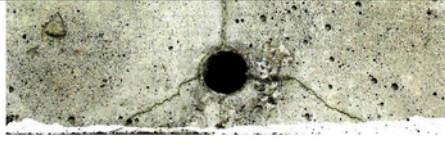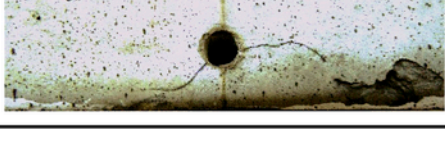
Concrete ID	Concrete cover 10 mm
	Crack pattern
C1	
C2	
C3	
C4	

Fig. 19. Top view of specimens after pull-out of the GFRP ⌀8 bar, for concretes C1 – C4 and cover of 10 mm.

eccentric pull-out specimens comparing to typical centric ones, especially pronounced for lower strength concretes. Higher bond strength, lower slip values, progressive bond failure, but also cracking of concrete cover and brittle post-peak bond behaviour are features of these eccentric tests. Other researchers have shown similar, higher bond strength and lower slip values with eccentric tests ([29] [30]), although with different type of FRP bar (sanded and spirally wrapped) and different type of test setup.

Measured slip values, DIC recording and photos gave better understanding of bond failure mode in eccentric specimens. With lower concrete cover and higher concrete strength bar was more capable for developing progressive ('zipper type' [10]) bond failure mode, with uneven bond-stress distribution along embedment length. On contrary, with increasing of confinement and lowering of concrete strength the bond behaviour was more "ductile".

As explained in Ref. [31], if the rib face angles are larger than 40° (here is 50°), slip is almost completely due to the crushing of the porous concrete paste (mortar) in front of the bar ribs. Having a look of Fig. 17, it is noticeable almost complete absence of concrete in-between bar ribs for centric specimens. Namely, due to presence of confinement forces (resulting from concrete around the centric bars) and absence of splitting displacement, low strength concretes' corbels collapse under the compressive forces and become incapable to hold the bar and attain bond strength as big as in case of eccentric specimens. In the beginning of loading process, centric bond shows indication of progressive debonding along embedment length (Fig. 14c). Further on, the concrete between ribs is starting being damaged. With all concrete corbels slightly damaged, bar begins to slide, even before reaching maximum bond stress. This is supported by Fig. 14c (specimens G8C1_c and G8C2_c), showing free- and loaded-end slips having almost constant difference before reaching peak stress. The resistance of confined concrete engages bar surface in bearing, so it is scratched after pull-out (Fig. 17), but still not sufficiently to produce significant influence on bond behaviour. The final failure of corbels occurs when bond reached its maximum stress level, which is fol-

lowed by descending phase of bond stress based on residual friction between bar and concrete. Post-peak branch of τ-slip curve is therefore not abrupt, as in case of eccentric specimens, since great part of corbels' crushing is already completed in pre-peak phase.

Therefore, confinement seems to have negative influence on the bond strength of this type of GFRP bars. Increase of confinement not only affect the overall stress in concrete cover, but also influence the redistribution of stress between bar and concrete, which can lead to change of failure mode from direct concrete splitting to crushing of concrete corbels and in some cases, decrease of bond strength with increase of concrete cover.

When higher strength concrete is used (e.g. C3), this phenomenon is not so evident and cannot be treated as a rule.

Tests performed with the same type of GFRP bars showed higher bond strength for beam tests comparing to centric pull-out tests [32], opposite to standard steel bars in same conditions. This underlines the importance of eccentric pull-out test for better estimating real bond performance of this type of bars when planned to be used in structural elements.

5. Conclusions

Presented paper investigated the bonding behaviour between two different types of GFRP bars and concrete, and made comparison with corresponding standard steel bars. Beside bars' material and external surface, eccentric and centric pull-out tests were designed to measure the effect of concrete mechanical properties and position of the bar in the concrete specimen (effect of concrete cover). DIC analysis gave the better insight into cracks' development pattern, suggesting the onset of cracking and debonding behaviour. Therefore, eccentric tests provided better understanding of the bonding mechanisms and crack development patterns that were described in details. The main results of the experimental investigation suggest some conclusions and practical recommendations.

- Sanded and spirally wrapped GFRP bars ⌀6 demonstrated brittle bond behaviour with sudden debonding of whole sand coating layer, but they also showed capability to develop continual debonding process, even when high strength concrete is used.
- Ribbed GFRP bars ⌀8 developed outwardly similar bond behaviour to steel counterparts, but with different debonding mechanism. These GFRP bars required almost 30% more fracture energy during debonding process.
- Both types of GFRP bars presented comparable, but still, in average, lower bond strength compared to steel ones under the same experimental conditions. Use of thin concrete cover (10 mm in this case) in combination with ribbed GFRP bars attained similar bond strength as steel bars and showed the real advantage of use of this GFRP bars instead of standard steel ones.
- Ribbed GFRP bars develop bond strength differently according to concrete mechanical properties. Concretes with average compressive strength in range 25–40 MPa do not influence strongly the bond strength, while within range of 40–65 MPa, bond strength is enhancing significantly. Highest concrete strength delays onset of cracking in low covers, but allows smoother and faster crack advancement.
- Ribbed GFRP bar developed higher bond strength and lower slip values in case of eccentric pull-out specimens, comparing to typical centric ones. This occurrence is especially pronounced for lower strength concretes. The main reason for this behaviour is GFRP bars' low splitting tendency and low width of concrete corbels.
- Combination of mid-strength concrete (55 MPa) with low concrete cover 10–15 mm appears to be preferable for present ribbed GFRP

rebars, since such combination of materials properties delays cover cracking and allows development of higher bond stresses.

GFRP ribbed bar overall showed very good bond behaviour, comparable to steel, indicating to be capable to replace it especially when low concrete cover/slender elements are used.

Finally, as the main intent of the present investigation is the understanding of GFRP bar-concrete bond behaviour, but with the aim of possible use for structural applications, the obtained results encourage use of eccentric pull-out test and provide a detailed dataset to assess the accuracy of refined numerical models (see e.g. Ref. [4]), as well as, analytical formulation for bond strength prediction available in some design recommendations. For this purpose, Fig. 20 presents the comparison of bond strength as measured in the present experimental investigation and predicted in some design codes, namely: ACI 440.1R [33] (ACI-1 and ACI-2 in Fig. 20), CSA-S806-12 [34] (CSA), CSA-S6-06 [35] (CHBDC) and Japanese recommendation [36] (JSCE). Those take into account, beside the concrete strength, the cover influence as well. The lowest and highest concrete qualities and two concrete covers adopted in this investigation were supposed for comparison. Several of the considered codes underestimate the bond strength compared to the experimental results and appear to be overly conservative. Only the ACI predicts bond strength of the GFRP bars close to the measured values in this experimental investigation. Similar observations are detailed in Ref. [37] for other GFRP bars and concrete qualities compared to beam test measurements.
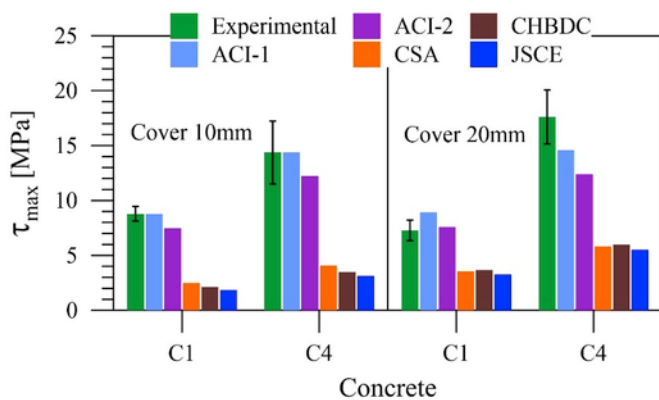
Acknowledgements

Fig. 20. Bond strength: Comparison of experimental and design recommendations.

References

[1] H.V.S. GangaRao, N. Taly, P.V. Vijay, Reinforced concrete design with FRP composites, CRC Press, Taylor & Francis Group, Boca Raton, FL, 2007.

[2] Technical Committee CEN/TC250, Eurocode 2: Design of concrete structures - Part 1-1: general rules and rules for buildings, CEN - European Committee for Standardization, Brussels, Belgium, 2004.

[3] S. Sólyom, G. L. Balázs and A. Borosnyói, "Bond behaviour of FRP rebars – parameter study," in Proceedings of SMAR 2015 The Third Conference on Smart Monitoring, Assessment and Rehabilitation of Civil Structures, Antalya, Turkey, September 2015.

[4] G. Fava, V. Carvelli, M. Pisani, Remarks on bond of GFRP rebars and concrete, Compos Part B 93 (2016) 210–220.

[5] RILEM TC9-RC, RC6-Bond test for reinforcement steel. 2. Pull-out test, 1983, In: RILEM recommendations for the testing and use of constructions materials, E & FN SPON, London, 1994, pp. 218–220.

[6] Fib Task Group Bond Models, "fib Bulletin 10 "Bond of reinforcement in concrete"," International Federation for Structural Concrete (fib)/Sprint-Druck, Lausanne, Switzerland/Stuttgart, Germany, 2000.

[7] E. Cosenza, G. Manfredi, R. Realfonzo, Behavior and modeling of bond of FRP rebars to concrete, J Compos Constr 1 (2) (1997) 40–51.

[8] H. Wang, A. Belarbi, Static and fatigue bond characteristics of FRP rebars embedded in fiber-reinforced concrete, J Compos Mater 44 (13) (2010) 1605–1622.

[9] M. Baena, L. Torres, A. Turon, C. Barris, Experimental study of bond behaviour between concrete and FRP bars using a pull-out test, Compos Part B 40 (8) (2009) 784–797.

[10] R. Tepfers, L. De Lorenzis, Bond FRP Reinf Concr — A Chall 39 (4) (2003) 477–496.

[11] A. Weber, "Bond Properties of a Newly Developed Composite Rebar," in Proceedings of the International Symposium on Bond Behaviour of FRP in Structures, Hong Kong, China, 2005, December 7 – 9.

[12] M.R. Ehsani, H. Saadatmanesh, S. Tao, Design recommendations for bond of GFRP rebars to concrete, J Struct Eng 122 (1996) 247–254.

[13] Hughes Brothers, Glass fiber reinforced polymer (GFRP) rebar - Aslan™ 100 series, November 2011. Available: http://www.aslanfrp.com/.

[14] ComBAR® Schöck, Schöck ComBAR glass fibre reinforcement - technical information, August 2013. Available: http://www.schoeck-combar.com/.

[15] ACI Committee 440, Guide test methods for fiber-reinforced polymers (FRPs) for reinforcing or strengthening concrete structures (ACI 440.3R-04), American Concrete Institute, 2004.

[16] Q. Hao, Y. Wang, Z. He, J. Ou, Bond strength of glass fiber reinforced polymer ribbed rebars in normal strength concrete, Constr Build Mater 23 (2) (2009) 865–871.

[17] M.M. Al-Zahrani, S.U. Al-Dulaijan, A. Nanni, C.E. Bakis, T.E. Boothby, Evaluation of bond using FRP rods with axisymmetric deformations, Constr Build Mater 13 (6) (1999) 299–309.

[18] Fib - Fédération internationale du béton, fib Bulletin No. 1-Textbook on Behaviour, Design and Performance, first ed., vol. 1, fib Fédération internationale du béton, 1999, p. 292.

[19] DIN, DIN 488–2: reinforcing steels - reinforcing steel bars, Deutsches Institut fur Normung E.V. (DIN), Berlin, Germany, 2009.

[20] CEN - European Committee for Standardization, EN 12390–3: 2009, Testing hardened concrete - Part 3: compressive strength of test specimens, CEN, Brussels, Belgium, 2009.

[21] CEN - European Committee for Standardization, EN 12390–6: 2009, Testing hardened concrete- Part 6: tensile splitting strength of test specimens, CEN, Brussels, Belgium, 2009.

[22] CEN - European Committee for Standardization, EN 12390–13: 2013, Testing hardened concrete - Part 13: determination of secant modulus of elasticity in compression, CEN, Brussels, Belgium, 2013.

[23] M. Sutton, J. Orteu, H. Shreir, Image correlation for shape, motion and deformation measurements: basic concepts, theory and applications, Springer Science, 2009.

[24] GOM mbH, "ARAMIS v6.3," GOM optical measuring techniques, 2011. Braunschweig, Germany.

[25] W.H. Soong, J. Raghavan, S.H. Rizkalla, Fundamental mechanisms of bonding of glass fiber reinforced polymer reinforcement to concrete, Constr Build Mater 25 (6) (2011) 2813–2821.

[26] M.A. Aiello, M. Leone, M. Pecce, Bond performances of FRP rebars-reinforced concrete, J Mater Civ Eng 19 (3) (2007) 205–213.

[27] Comite Euro-International Du Beton, CEB-FIP model code 1990: design code, Thomas Telford, London, England, 1993.

[28] D. Tasevski, Effect of surface treatment on the bond behaviour of Fiber Reinforced Polymer (FRP) reinforcement and concrete, In: Master of research

SMCD 'material science for sustainable construction', Ecole des Ponts, Lafarge, Paris, France, 2013.

[29] R. Tepfers, G. Hedlund and B. Rosinski, "Pull-out and Tensile Reinforcement Splice Tests with GFRP Bars," in Proceedings of 'Second International Conference on Composites in Infrastructure', Tucson, Arizona, 1998.

[30] N. Galati, A. Nanni, L.R. Dharani, F. Focacci, M.A. Aiello, Thermal effects on bond between FRP rebars and concrete, Compos Part A 37 (8) (2006) 1223–1230.

[31] L.A. Lutz, P. Gergely, Mechanics of bond and slip of deformed bars in concrete, ACI Struct J 64 (11) (1967) 711–721.

[32] E. Gudonis, R. Kacianauskas, V. Gribniak, A. Weber, R. Jakubovskis, G. Kaklauskas, Mechanical properties of the bond between GFRP reinforcing bars and concrete, Mech Compos Mater 50 (4) (2014) 457–466.

[33] ACI Committee 440, Guide for the design and construction of structural concrete reinforced with FRP bars (ACI 440.1R-15), American Concrete Institute, Farmington Hills, MI, 2015.

[34] Canadian Standards Association (CSA), Design and construction of building structures with fibre-reinforced polymers (CSA-S806-12), 2012. Mississauga, Canada.

[35] Canadian Standards Association (CSA), Canadian highway bridge design code (CAN/CSA-S6-06), 2006. Mississauga, Canada.

[36] Japan Society of Civil Engineers (JSCE), Recommendation for design and construction of concrete structures using continuous fiber reinforcing materials, 1997.

[37] F. Yan, Z. Lin, M. Yang, Bond mechanism and bond strength of GFRP bars to concrete: a review, Compos Part B 98 (2016) 56–69.